High single-cell diversity in carbon and nitrogen assimilations by a chain-forming diatom across a century

Malin Olofsson [ID],[1]* **Olga Kourtchenko**,[1]
Eva-Maria Zetsche,[1] **Hannah K. Marchant** [ID],[2]
Martin J. Whitehouse,[3] **Anna Godhe**[1] and
Helle Ploug[1]

[1]*Department of Marine Sciences, University of Gothenburg, Box 461, 405 30, Gothenburg, Sweden.*
[2]*Max Planck Institute for Marine Microbiology, Celsiusstrasse 1, 28359, Bremen, Germany.*
[3]*Swedish Museum of Natural History, Box 50 007, 104 05, Stockholm, Sweden.*

Summary

Almost a century ago Redfield discovered a relatively constant ratio between carbon, nitrogen and phosphorus in particulate organic matter and nitrogen and phosphorus of dissolved nutrients in seawater. Since then, the riverine export of nitrogen to the ocean has increased 20 fold. High abundance of resting stages in sediment layers dated more than a century back indicate that the common planktonic diatom *Skeletonema marinoi* has endured this eutrophication. We germinated unique genotypes from resting stages originating from isotope-dated sediment layers (15 and 80 years old) in a eutrophied fjord. Using secondary ion mass spectrometry (SIMS) combined with stable isotopic tracers, we show that the cell-specific carbon and nitrogen assimilation rates vary by an order of magnitude on a single-cell level but are significantly correlated during the exponential growth phase, resulting in constant assimilation quota in cells with identical genotypes. The assimilation quota varies largely between different clones independent of age. We hypothesize that the success of *S. marinoi* in coastal waters may be explained by its high diversity of nutrient demand not only at a clone-specific level but also at the single-cell level, whereby the

population can sustain and adapt to dynamic nutrient conditions in the environment.

Introduction

Picturing an ocean in homeostasis, Redfield made pioneering discoveries, which revealed a close relationship between nutrient ratios in organic matter and seawater. This relationship led to the theory of a fixed stoichiometric ratio between carbon, nitrogen and phosphorus (106:16:1) in phytoplankton based on the ratio at which the nutrients are consumed by phytoplankton during growth (Redfield, 1934; 1958). Throughout the last decades, this concept has been reconsidered based on culture studies indicating large variations in organic matter nutrient ratios, associated to nutrient availability, light and temperature (Geider and LaRoche, 2002; Gruber and Deutch, 2014; Garcia *et al*., 2018). Since the introduction of fertilizers within the agroindustry during the last century, concentrations of nitrate, particularly in coastal areas, have increased. Riverine fluxes of nitrogen to the ocean are estimated to have increased 2- to 20-fold since preindustrial times (Howarth *et al*., 1996; Conley *et al*., 2000; Clarke *et al*., 2006). These anthropogenic changes are predicted to affect the global nitrogen budget in a future ocean (Gruber and Deutch, 2014; Hutchins and Fu, 2017) and may ultimately change the conceptual carbon-to-nitrogen ratio of algal cells in the ocean.

Chain-forming diatoms are key organisms in the biological fixation and sequestration of CO_2 in the ocean (Nelson *et al*., 1995; Bergkvist *et al*., 2018). In the euphotic zone, they form fast-sinking aggregates, which transport fixed inorganic carbon and nutrients to the deep sea or shallow sediments (Fowler and Knauer, 1986; Alldredge and Gotschalk, 1988). Shallow, coastal sediments receive large inputs of organic matter due to eutrophication and increased primary production in surface waters (Diaz and Rosenberg, 2008). The cosmopolitan diatom genus *Skeletonema* is a key primary producer during spring blooms in temperate seas, where it assimilates nitrate at high rates compared to ammonium (Godhe *et al*., 2016; Bergkvist *et al*., 2018). As a part of

its life cycle, *Skeletonema* forms resting stages in the sediment when growth conditions in the photic zone are unfavourable. The high abundance of *Skeletonema* resting stages in coastal sediments (up to 50,000 g^{-1} sediment), and their presence in sediment layers dating more than a 100 years back, demonstrates that these diatoms have sustained their presence and durability in spite of highly variable growth conditions (McQuoid *et al*., 2002). These resting stages can survive for at least a century in the sediment, and upon revival, we can study adaptations to eutrophication within local *Skeletonema* populations (McQuoid *et al*., 2002; Härnström *et al*., 2011; Ellegaard *et al*., 2018). A recent study demonstrated higher variability of diatoms in carbon, nitrogen and phosphorus quota on a clone specific level compared to other phytoplankton (Garcia *et al*., 2018). We hypothesized that a diversity of nutrient demands occurs even at a single-cell level in diatoms including *Skeletonema.*

To test this hypothesis, we applied secondary ion mass spectrometry (SIMS) in combination with stable isotopic tracers to measure carbon and nitrate assimilations on revived resting stages of *Skeletonema marinoi*, originating from a fjord with increased eutrophication (especially of nitrate), during the last century (Ellegaard *et al*., 2006). Hereby, we could analyse carbon and nitrate assimilation rates and their ratios on a single-cell level across various clones and across a time span encompassing 30,000 generations of this diatom in its natural environment.

Results and discussion

By reviving resting stages (80 and 15 years) of the common diatom *S. marinoi* from the Danish Mariager Fjord and quantifying their assimilation rates of carbon and nitrate, we revealed the dynamics of carbon-to-nitrate assimilation ratio and nutrient demands at both the clonal and single-cell level back to the time of Redfield. Current winter nitrate concentrations in this fjord are at 90 μM prior to the spring bloom (Sildever *et al*., 2016). The monoclonal isolates, established from recently revived single resting stages, were incubated under both nitrate-replete conditions (nitrate was replete while phosphate and silicate concentrations were depleted in the stationary growth phase) and nitrate-limited conditions (nitrate was nondetectable while phosphate concentrations were replete in the stationary growth phase) (Supporting Information Fig. S1). Experiments applying stable isotopic tracers were conducted during exponential, stationary and late stationary growth phases (Supporting Information Fig. S2).

An example of SIMS and isotope ratio images of *Skeletonema* cells is shown in Fig. 1. Cell-specific carbon and nitrate assimilation rates were derived from the isotope ratio images (Eqs. 1 and 2) and are shown in Fig. 2. The cell-specific carbon and nitrate assimilation rates at single-cell level varied up to one order of magnitude and were significantly correlated resulting in stable carbon to nitrate assimilation quota across the individual cells within the same clone during the exponential growth phase (Fig. 2A, B, D, E, G, and H). These correlations disappeared during the stationary growth phase when the assimilation rates decreased and carbon-to-nitrate assimilation ratios increased well above the Redfield ratio (Fig. 2C, F and I and Fig. 3). Recently, a similar variation of carbon and nitrate assimilation rates at a single-cell level was reported in two field populations of chain-forming diatoms (*Skeletonema* and *Chaetoceros*) during a spring bloom (Bergkvist *et al*., 2018). In those field populations, the individual cell-specific carbon and nitrate assimilation rates varied even more than one order of magnitude while the average carbon-to-nitrate assimilation ratio was close to the Redfield ratio, and ammonium assimilation rates were only 14% of nitrate assimilation rates. Hence, the overall variations observed in field population of chain-forming diatoms are presumably explained by variation on both the clonal and single-cell levels.

The cell-specific carbon and nutrient demand and assimilation rates depend on both cell size and growth rates. In diatoms, the cell size varies over generations due to their mitotic life cycle, with a decrease in cell diameter following each cell division, until eventually sexual reproduction is needed to restore the original cell size (Godhe *et al*., 2014). In the present study we observed a large variation in cell size across experiments and clones (Supporting Information Fig. S3). The variability of carbon and nitrate assimilation rates across the clones, however, did not decrease when the rates were normalized to the average cell volume measured within each clone (Fig. 2D and E). Instead, different intrinsic growth rates and slightly different growth phases may explain the large variation in assimilation rates. We calculated the specific growth rates of the carbon and nitrogen contents within single cells directly from the excess isotope ratios measured by SIMS, in order to normalize to variable cell size and biomass (Eq. 3). The results show a relatively decreased variability of, especially, carbon growth rates (Fig. 2G and H). Several clones, however, showed significantly different carbon and nitrogen growth rates during the exponential growth phase, independent of initial nutrient conditions (Table 1 and Supporting Information Table S1).

The variation in nitrate assimilation was substantially larger than the variation in carbon assimilation in all clones (Fig. 2 and Supporting information Tables S1 and S2). The carbon growth rate derived from SIMS measurements in single cells was similar to the relative increase in particulate organic carbon (POC) measured by EAIRMS in the exponential growth phase. In contrast, the nitrogen growth rates were highly variable within and between clones, and the clone-specific average value
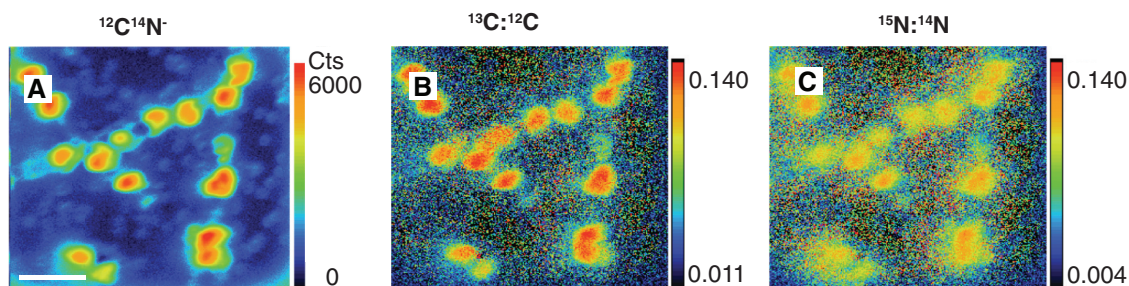
Fig. 1. SIMS images of *Skeletonema marinoi* cell chains. The biomass distribution is demonstrated by the $^{12}C^{14}N^-$ image (A) where the unit represents counts per pixel. SIMS images of $^{13}C{:}^{12}C$ ratio (B) and $^{15}N{:}^{14}N$ ratio reflect carbon and nitrate assimilations respectively. The scale bar represents 20 μm. [Color figure can be viewed at wileyonlinelibrary.com]
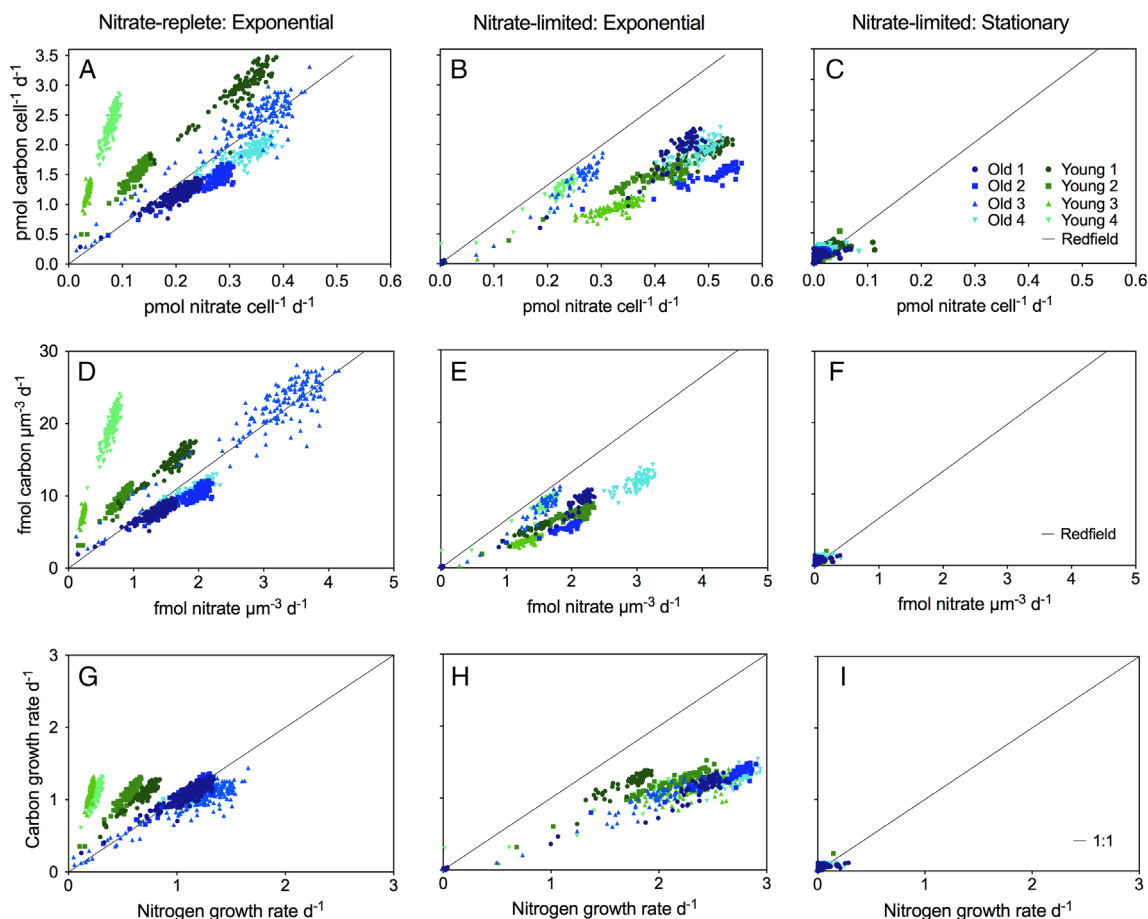

Fig. 2. Single-cell assimilation rates from SIMS analyses. The cell-specific carbon and nitrate assimilations in pmol cell^{-1} day^{-1} (A–C) and fmol μm^{-3} day^{-1} (D–F) and carbon- and nitrogen-specific growth rates day^{-1} (G–I), during nitrate-replete conditions (A, D and G) and nitrate-limited conditions (B, C, E, F, H and I), for all strains during exponential growth phase (A, B, D, E, G and H) and stationary growth phase (C, F and I). Black lines indicate either Redfield ratio (A–F) or 1:1 ratio (G–I). [Color figure can be viewed at wileyonlinelibrary.com]

was higher than the measured particulate organic nitrogen (PON) increase during the exponential growth phase (Supporting Information Table S1). This may suggest that a pool of organic nitrogen within the vacuole of diatoms was growing fast but did not quantitatively dominate the total particulate organic nitrogen (PON). Nitrate was assimilated into biomass earlier relative to carbon prior to

the stationary phase in several clones across the various ages (Supporting Information Figs S1, S4 and S6 and Tables S3–S5). *Skeletonema marinoi* is able to store nitrate intracellularly, exceeding extracellular concentrations by orders of magnitude (Kamp *et al*., 2016), and the assimilation rate may substantially increase when nitrate concentrations are above 50–100 μM, suggesting an

Table 1. The ratio (column:row) of carbon- and nitrogen-specific growth rates day^{-1} under nitrate-replete and nitrate-limited conditions during exponential growth phase between young (Y) and old (O) clones. [Color table can be viewed at wileyonlinelibrary.com]

		Nitrate-replete								Nitrate-limited							
		Y1	Y2	Y3	Y4	O1	O2	O3	O4	Y1	Y2	Y3	Y4	O1	O2	O3	O4
Carbon growth rate d^{-1}	Y1	-	1.00	**1.06**	1.02	1.00	1.05	**0.91**	1.02	-	0.98	**0.94**	**0.90**	**0.83**	1.05	**0.75**	1.03
	Y2		-	**1.06**	1.01	1.00	1.05	**0.91**	1.02		-	0.96	0.92	**0.84**	**1.07**	**0.76**	1.05
	Y3			-	0.96	**0.95**	0.99	**0.86**	**0.96**			-	0.96	0.88	**1.12**	**0.80**	**1.10**
	Y4				-	0.99	1.03	**0.90**	1.00				-	0.92	**1.16**	**0.83**	**1.14**
	O1					-	**1.05**	**0.91**	1.02					-	**1.27**	0.91	**1.25**
	O2						-	**0.87**	0.97						-	**0.71**	0.98
	O3							-	**1.12**							-	**1.37**
	O4								-								-
Nitrogen growth rate d^{-1}	Y1	-	**0.81**	**0.30**	**0.38**	**1.60**	**1.67**	**1.74**	**1.65**	-	**1.25**	**1.38**	**1.15**	**1.22**	**1.50**	1.06	**1.54**
	Y2		-	**0.37**	**0.47**	**1.99**	**2.07**	**2.17**	**2.05**		-	**1.11**	0.92	0.98	**1.21**	**0.85**	**1.24**
	Y3			-	**1.26**	**5.32**	**5.54**	**5.80**	**5.50**			-	**0.83**	0.88	**1.09**	**0.77**	**1.12**
	Y4				-	**4.23**	**4.40**	**4.61**	**4.37**				-	1.06	**1.31**	0.92	**1.34**
	O1					-	1.04	1.09	1.03					-	**1.24**	0.87	**1.27**
	O2						-	1.05	0.99						-	**0.71**	1.03
	O3							-	0.95							-	**1.45**
	O4								-								-

Colours range from low values in dark green to high values in red. Bold numbers indicate significant differences between clones (*p*-value < 0.05). The growth rates are derived from single-cell measurements (SIMS) with $N = 57–265$. Welch ANOVA and Games-Howell.

active uptake system adapted to high concentrations (Collos *et al.*, 1992). Such luxury uptake may have occurred prior to our measurements in the clones showing low nitrogen growth relative to carbon growth under nitrate-replete conditions. Using SIMS, we measured organic matter as carbon-nitrogen compounds, for example, urea, rather than nitrate stored in the vacuole. Such reduction of

Fig. 3. Single-cell assimilation rates from SIMS analyses. The cell-specific carbon and nitrate assimilations in pmol cell^{-1} day^{-1} during nitrate-limited conditions for all strains during stationary growth phase. Black line indicate Redfield ratio. [Color figure can be viewed at wileyonlinelibrary.com]

nitrate and assimilation into urea may also occur during high nitrogen growth. Nitrate reductase combined with the ornithine-urea cycle supports urea as nitrogen storage product in diatoms and has been suggested to be key to the evolutionary success of diatoms (Bowler *et al.*, 2008; Allen *et al.*, 2011; McCarthy *et al.*, 2017). This trait may indeed be advantageous in environments with highly dynamic nutrient sources and may also partly explain the large variation of nitrate assimilation rates observed at both clone-specific and cell-specific level.

The exponential, nutrient-replete phase in our experiments lasted 2–3 days, only, while the nutrient-limited growth early stationary phase was almost linear and lasted 1–2 weeks depending on the initial nutrient concentrations (Supporting Information Fig. S2). The carbon doubling time calculated from the carbon growth rates derived from SIMS as well as from the observed increase in POC, and the relative increase in fluorescence, was less than 1 day during the exponential growth phase independent of initial nutrient concentrations (Fig. 2 and Supporting Information Fig. S2 and Table S5). During the stationary growth phase, the carbon doubling time increased to 10–13 days under nitrate-limited conditions. By comparison, a carbon doubling time of 5 days in *Skeletonema* indicated its transition into the early stationary growth phase under low
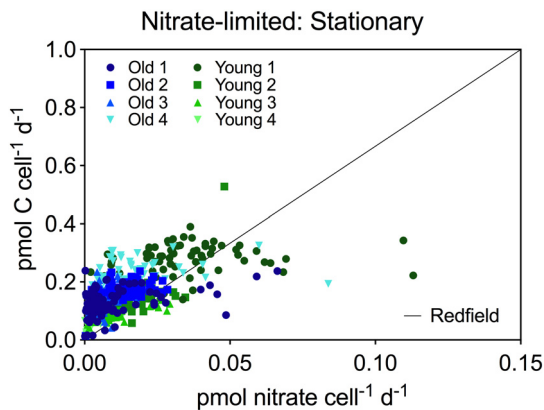
(< 0.3 μM) nitrate concentrations during a spring bloom in the Baltic Sea (Bergkvist *et al.*, 2018).

During stationary growth under nitrate-limited conditions, the variation in specific growth rates within each clone was similar to the overall variation of specific growth rates for pooled clones (Supporting Information Table S2). Interestingly, a few cells assimilated carbon and nitrogen at relatively high rates when the majority of cells had entered the stationary growth phase (Fig. 3). Such cells show high fitness to low nutrient concentrations and may sustain growth into the summer when nutrient concentrations and diatom abundances are low in the field. SIMS studies of phytoplankton communities during early summer have shown that carbon doubling times can be relatively high (ca. 3 days) in another chain-forming diatom (*Chaetoceros* sp.) even when dissolved inorganic nitrogen concentrations were ~ 0.5 μM (Adam *et al.*, 2016).

During the present study, the cells chain^{-1} decreased significantly from up to 14 cells chain^{-1} down to three cells chain^{-1} during the transition from the exponential to the stationary growth phase (Supporting Information Fig. S5). Ion transporters limit the nutrient uptake across the cell membrane (reaction limitation) under nutrient-replete conditions and exponential growth, whereas diffusion and turbulent shear can limit transport of nutrients to the cell membrane under nutrient-limiting conditions. *Skeletonema* forms long cell-chains both in cultures and in the field (up to 22 cells chain^{-1}) (Bergkvist *et al.*, 2012; 2018; Sildever *et al.*, 2016). Such long cell chains are beneficial for growth in a turbulent environment, and carbon assimilation rate in *Skeletonema* increased by about 30% at a turbulence level equal to that occurring in the wave breaking zone when nitrate concentrations were < 0.3 μM (Bergkvist *et al.*, 2018). Turbulence was absent during the present study. Hence, *Skeletonema* may reduce its chain length to increase its surface to volume ratio and alleviate diffusion limitation when nutrient concentrations are low and turbulence is absent, as was the case in the present study.

Previous studies have described large phenotypic and genetic variation among *Skeletonema* clones (Kremp *et al.*, 2012; Sjöqvist and Kremp, 2016; Gross, 2017). In the present study, we have further magnified the analytical resolution by identifying the diversity of thousands of individual cells within and across clones spanning almost a century in time using novel approaches. Examining Redfield's concept of relative fixed stoichiometric ratios (Redfield, 1934; 1958) we have demonstrated that the carbon-to-nitrate assimilation ratios at the single cell level is highly variable and often far from Redfield. However, carbon-to-nitrogen ratios in biomass at the clonal level averaged for thousands of cells were much closer to the actual Redfield ratio (Supporting Information Table S3). Interestingly, this diversity at a single-cell level was age independent suggesting a large diversity in carbon-to-

nitrate assimilation ratios also 80 years ago. The cell-specific assimilation rates varied more between clones of the same age than across clones from different time periods. This observation further inflates the already documented enormous genetic standing stock of diatom bloom populations (Rynearson and Armbrust, 2005; Chen and Rynearson, 2016). Such diversity on cellular level can provide resilience to variations in the environment, for example nutrient availability, and contributes to the success of diatom populations in diverse environments. We hypothesize that this large diversity and variation in nutrient demands among single cells within clones is the key for the success of the diatoms to be resilient during eutrophication and when dispersing into new areas.

Experimental procedures

Experimental design

We conducted the following three separate experiments using f/8-media (Guillard, 1975) with modified nitrate conditions to test the sensitivity to nitrate availability in *S. marinoi*: (i) nitrate-replete conditions (200 μM), (ii) nitrate-limited conditions (50 μM) and (iii) nitrate-limited conditions (60 μM) at higher time resolution to evaluate luxury uptake in the exponential growth phase under nitrate limitation. In the first two experiments, eight recently revived clones germinated from resting stages of the diatom *S. marinoi* from the Danish Mariager Fjord were used. Four clones originated from young (15 years) and four clones originated from old (80 years) isotope dated sediment layers (Härnström *et al.*, 2011). In a third experiment, seven additional clones were included, originating from germinated resting stages of the two sediment layers (15 and 80 years). All resting stages were revived in f/8 media, prepared from water collected via deep-water intake (prefiltered 0.45 μm, followed by 0.2 μm) at Sven Lovén Centre for Marine Sciences, Kristineberg (58°25′N, 11°44′E) in March 2016. The salinity of the water was adjusted to 26 with MilliQ. To establish unique genotypes, one cell-chain from each well was isolated by micropipetting and grown as a separate clone (details in Härnström *et al.*, 2011). Prior to the inoculation to the experiments, the clones had 1 week of acclimation in the modified media, at experimental temperature and light conditions. At day 0 of the first two experiments, five replicates of each clone and, in the nitrate-limited high-resolution condition, three replicates of each clone were inoculated into 650 ml culture bottles (~ 3000 cells ml^{-1}) and kept at 11/13°C (night/day) in a 12:12 h light:dark (9 am to 9 pm) cycle (75 μmol photons m^{-2} s^{-1}, PAR, measured with a LiCOR irradiance sensor).

With no bioturbation in anoxic sediments due to increased eutrophication during the last century, the

Mariager Fjord is suited to reveal possible effects on the diatom population (Ellegaard *et al.*, 2006). The present day winter nutrient concentrations in the fjord are 47 μM silicate, 90 μM nitrate and 3 μM ortho-phosphate, resulting in a dissolved inorganic nitrogen-to-phosphorus ratio of 30 (Sildever *et al.*, 2016). In all three experiments, the initial nitrate-to-silicate ratio of approx. 1.8 and nitrate-to-phosphate ratio of approx. 10–12, meant that according to Redfield, nitrate was slightly in excess of silicate and phosphate in excess of nitrate.

Growth and microscopy analysis

Growth curves were established by daily sampling of 700 μl for measurements of relative fluorescence unit (RFU) on multi-well plates using a Varioscan™ Flash Multimode Reader (ThermoScientific) with fluorescence settings at 425 nm excitation and 680 nm emission detection wavelengths. These measurements provide relative estimates of *in vivo* chlorophyll *a* concentrations (method further described in Gross *et al.*, 2018). Cell abundance and size were analysed by microscopy (Olenina *et al.*, 2006). Additional samples of 4 ml were fixed with Lugol's solution at day 0, and prior to the incubations during nitrate-replete and nitrate-limited conditions, as well as on days 4 and 6 of the third experiment. The number of cells chain^{-1} was counted using microscopy, continuing until a stable mean value and standard deviation were reached (approx. 60–80 chains). The microscopy analyses were performed at exponential and stationary growth phases under nitrate-limited conditions in samples fixed with paraformaldehyde and filtered onto TTTP filters.

Dissolved inorganic nutrients

On day 0, preceding the incubations with isotopic tracers, 7 ml were collected from each bottle using a syringe filter (0.2 μm) and immediately stored frozen (−20°C) until further analysis. Concentrations of dissolved inorganic nutrients (ammonium, nitrite + nitrate, silicate and phosphate) were analysed according to Grasshoff and colleagues (1999) at Sven Lovén Centre for Marine Sciences, Kristineberg. During the high time resolution experiment with nitrate limitation, the nitrate concentration was analysed daily spectrophotometrically (Schnetger and Lehners, 2014).

Stable isotope incubations

The 24-h incubations with stable isotope tracers were carried out to measure cell- and clone-specific carbon and nitrate assimilation rates. Initiation of the incubations was decided based on the RFU data, where the exponential (nutrient replete), early stationary (nutrient limited) and late stationary (decaying growth) phases were identified. The cells were still growing during stationary growth phase (Supporting Information Fig. S2c and d). The bottles with the individual clones were labelled with ^{13}Carbon bicarbonate (Sigma-Aldrich) (6.7%–8.5% excess labeling) and ^{15}N nitrate (Sigma-Aldrich) (0.8%–12.6% excess labeling) and experiments and analysis were conducted according to Montoya and colleagues (1996) and Füssel and colleagues (2012). Incubations with stable isotope tracers were performed in 160 ml gas tight serum bottles (15°C, 100 μmol photons m^{-2} s^{-1}, 24 h from 9 am). ^{15}N nitrate labeling % was determined by comparing the concentration of ^{15}N nitrate to total (^{14}N + ^{15}N) nitrate concentrations. The concentration of ^{15}N nitrate was analysed by GC-IRMS coupled to an IsoPrime100 (Manchester, UK) according to Füssel and colleagues (2012) in Bremen, Germany. The ^{13}C labeling % of dissolved inorganic carbon (DIC) was analysed by Picarro (Cavity ring down Spectrometer G2201-I coupled to an Isotopic CO2/CH4 IRMS, Liaison A0301) according to Torres and colleagues (2005) in Bremen, Germany.

Clone-specific analyses

The stable isotope incubations were terminated by filtering samples onto precombusted (450°C) GF/F filters (Montoya *et al.*, 1996). The filters were first dried (60°C, overnight) and then decalcified by exposure to HCl fumes overnight in a glass desiccator, before being packed into tin cups. The samples were analysed for the incorporation of ^{15}N nitrate into PON and ^{13}C bicarbonate into POC by Elemental Analysis Isotope ratio mass spectrometry (EA-IRMS) at the Department of Geology, University of Gothenburg. Samples for particulate organic phosphorus were collected on GF/F filters during the last incubations of nitrate-replete and nitrate-limited conditions and analysed using ICP Emission spectroscopy on an iCAP 6500 (Thermo Scientific) at the Royal Netherlands Institute for Sea Research, the Netherlands. One-way ANOVA was used (SPSS Statistics Version 20) to compare old against young clones when pooled together ($N = 20$, $p < 0.05$). Levene's test was used to check for homogeneity, and Welch ANOVA was used when the variations were heterogeneous. EA-IRMS analysis was completed before SIMS analysis was initiated. The replicates of cell-specific carbon and nitrogen assimilation rates subsequently measured by SIMS were selected from the bottles with community nitrate assimilation rates closest to the mean value of the nitrate assimilation measured by EAIRMS.

Cell-specific analyses

Before and at the end of the incubations with stable isotopic tracers, 5 ml of sub-samples were preserved with 1% paraformaldehyde and stored in the dark (4°C, 24 h). The samples were thereafter filtered onto TTTP filters (pore size 2.0 μm), washed with phosphate-buffered saline [PBS (10×), pH 7.4]

and stored at room temperature until analysis. ^{13}C and ^{15}N incorporation into single cells of *S. marinoi* was analysed using SIMS on a large-geometry CAMECA (Gennevilliers, France) IMS 1280 instrument at the Swedish Museum of Natural History Museum in Stockholm, Sweden. The TTTP filters were cut into 4 mm × 4 mm pieces and glued onto glass slides and, thereafter, coated with a thin (ca. 10 nm) layer of gold. Areas of interest (80 μm × 80 μm) on the filters were pre-sputtered with a caesium ($^{133}Cs^+$) primary ion beam (10 nA) to remove the silicate frustule. A $^{12}C^{14}N^-$ signal in the frustule is hardly detectable, and the presputtering was continued until the $^{12}C^{14}N^-$ signal was maximal which occurred after 300 s. Thereafter, we used a nominal 50 pA analytical beam with a spatial resolution of ca. 1 μm to analyse the cell interior with its high carbon and nitrogen content. The dynamic transfer optical system applied a synchronized raster in the secondary beam to retain high-mass resolution capability. Following secondary beam optimization (centering in the field aperture, energy and mass calibration adjustment using the abundant $^{12}C^{14}N$ species), image analysis comprised 80 cycles through the species $^{12}C^{14}N$ (1 s. integration), $^{13}C^{14}N$ (5 s) and $^{12}C^{15}N$ (2 s), with a total analytical time of ca. 800 s. The use of carbon–nitrogen isotopomers have the advantage that they represent organic matter, they are bright, and two isotope ratios can be determined from measurements of three isotopomers. A mass resolution of 12,000 ($M/\Delta M$) was used to ensure adequate resolution of $^{13}C^{14}N$ from potentially interfering $^{11}B^{16}O$ (Zinner *et al.*, 1989) from the diatom frustule (Mejía *et al.*, 2013). Secondary ion images (256 × 256 pixels) were recorded for each species, with image data processing done using the WinImage2 software (CAMECA). Individual cells were defined as regions of interest (ROIs) on the $^{12}C^{14}N$ images (Fig. 1), from which the cell-specific isotope ratios $^{13}C/^{12}C$ and $^{15}N/^{14}N$ were derived. In total approx. A total of 2400 individual cells were analysed by SIMS. One-way ANOVA and post hoc tests (Tukey or Games-Howell) were used to reveal differences in cell-specific assimilation rates (SPSS Statistics Version 20).

Carbon and nitrate assimilation rates

The clone-specific carbon assimilation rates (nM day^{-1}) were calculated from the ^{13}C-atom% excess of DIC in the ambient water and the change in excess isotopic composition of organic matter during the incubation time, t measured by EAIRMS (Montoya *et al.*, 1996):

$$\text{Carbon assimilation rate} = \frac{\Delta 13C-\text{atom\%excess}_{(POC)} \times POC}{13C-\text{atom\%excess}_{(DIC)} \times \Delta t}$$

(1)

The cell-specific carbon assimilation rates were calculated analogously from the average POC per cell derived from the measured POC concentration divided by cell abundance and the change in ^{13}C-atom% excess isotopic composition of single cells during the incubation time, t, measured by SIMS (Bergkvist *et al.*, 2018).

The clone-specific nitrate assimilation rates (nM day^{-1}) were calculated from the ^{15}N-atom% excess of nitrate in the ambient water and the change in excess isotopic composition of organic matter during the incubation time, t, measured by EAIRMS (Montoya *et al.*, 1996):

$$\text{Nitrate assimilation rate} = \frac{\Delta 15N-\text{atom\%excess}_{(PON)} \times PON}{15N-\text{atom\%excess}_{(nitrate)} \times \Delta t}$$

(2)

The cell-specific nitrate assimilation rates were calculated analogously from the average PON per cell derived from the measured PON concentration divided by cell abundance and the change in ^{15}N-atom% excess isotopic composition of single cells during the incubation time, t, measured by SIMS (Bergkvist *et al.*, 2018).

The carbon growth rates (day^{-1}) and the nitrogen growth rates (day^{-1}) of the cell biomass were calculated from SIMS measurements of excess isotope ratios of ^{13}C:^{12}C and ^{15}N:^{14}N assuming an even distribution of the isotope in the biomass during cell division:

$$\text{C- or N-based growth rate (day}^{-1}) = (IR_{excess}/IR_{excess\text{-}label}) \times 2 \times 1/t$$

(3)

where IRxcess represents the excess isotope ratio of organic matter with respect to ^{13}C or ^{15}N, IRxcess-label represents the excess isotope ratio of DIC or nitrate during the incubation and t is the incubation time. The factor of 2 describes the dilution of the heavy isotope during assimilation into organic matter with an original isotope composition equal to the natural background during cell division.

References

Adam, B., Klawonn, I., Svedén, J. B., Bergkvist, J., Nahar, N., Walve, J., *et al*. (2016) N$_2$-fixation, ammonium release, and N-transfer to the microbial and classical food web within a plankton community. *ISME J* **126**: 1–10.

Alldredge, A. L., and Gotschalk, C. (1988) In situ settling behavior of marine snow. *Limnol Oceanogr* **33**: 339–351.

Allen, A. E., Dupont, C. L., Oborník, M., Horák, A., Nunes-Nesi, A., McCrow, J. P., *et al*. (2011) Exosymbiont-derived urea cycle used for intracellular carbon and nitrogen recovery in diatoms. *Nature* **473**: 203–207.

Bergkvist, J., Thor, P., Jakobsen, H. H., Wängberg, S.-Å., and Selander, E. (2012) Grazer-induced chain length plasticity reduces grazing risk in marine diatom. *Limnol Oceanogr* **57**: 318–324.

Bergkvist, J., Klawonn, I., Whitehouse, M. J., Lavik, G., Brüchert, V., and Ploug, H. (2018) Turbulence simultaneously stimulates small- and large-scale CO$_2$ sequestration by chain-forming diatoms in the sea. *Nat Commun* **9**: 3046.

Bowler, C., Allen, A. E., and Grigoriev, I. V. (2008) The *Phaeodactylum* genome reveals the evolutionary history of diatom genomes (2008). *Nature* **456**: 239–244.

Chen, G., and Rynearson, T. (2016) Genetically distinct populations of a diatom co-exist during the North Atlantic spring bloom. *Limnol Oceanogr* **61**: 2165–2179.

Clarke, A. L., Weckström, K., Conley, D. J., Anderson, N. J., Adser, F., Andrén, E., *et al*. (2006) Long-term trends in eutrophication and nutrients in the coastal zone. *Limnol Oceanogr* **51**: 385–397.

Collos, Y., Siddiqi, M. Y., Wang, M. Y., Glass, A. D. M., and Harrison, P. J. (1992) Nitrate uptake kinetics by two marine diatoms using the radioactive tracer ^{13}N. *J Exp Mar Biol Ecol* **163**: 251–260.

Conley, D. J., Kaas, H., Mølenberg, F., Rasmussen, B., and Windolf, J. (2000) Characteristics of Danish estuaries. *Estuaries* **23**: 820–837.

Diaz, R. J., and Rosenberg, R. (2008) Spreading dead zones and consequences for marine ecosystems. *Science* **321**: 926–929.

Ellegaard, M., Clarke, A. L., Reuss, N., Drew, S., Weckström, K., Juggings, S., *et al*. (2006) Multi-proxy evidence of long-term changes in ecosystem structure in a Danish Marine Estuary, linked to increase nutrient loading. *Estuar Coast Shelf Sci* **68**: 567–578.

Ellegaard, M., Godhe, A., and Ribiero, S. (2018) Time capsules in natural sediment archives-tracking phytoplankton population genetic diversity and adaptation over multidecadal timesclaes in the face of environmental change. *Evol Appl* **11**: 11–16.

Fowler, S. W., and Knauer, G. A. (1986) Role of large particles in the transport of elements and organic compounds through the oceanic water column. *Prog Oceanogr* **16**: 147–194.

Füssel, J., Lam, P., Lavik, G., Jensen, M. M., Holtappels, M., Günter, M., and Kuypers, M. M. M. (2012) Nitrite oxidation in the Namibian oxygen minimum zone. *ISME J* **6**: 1200–1209.

Garcia, N. S., Sexton, J., Riggings, T., Lomas, M. W., and Martiny, A. C. (2018) High variability in cellular stoichiometry of carbon, nitrogen, and phosphorus within classes of marine eukaryotic phytoplankton under sufficient nutrient conditions. *Front Microbiol* **9**: 543.

Geider, R. J., and LaRoche, J. (2002) Redfield revisited: variability of C:N:P in marine microalgae and its biochemical basis. *Eur J Phycol* **37**: 1–17.

Godhe, A., Kremp, A., and Montresor, M. (2014) Genetic and microscopic evidence for sexual reproduction in the centric diatom *Skeletonema marinoi*. *Protist* **165**: 401–416.

Godhe, A., Sjöqvist, C., Sildever, S., Sefbom, J., Hardardóttir, S., Bertos-Fortis, M., *et al*. (2016) Physical barriers and environmental gradients cause spatial and temporal genetic differentiation of an extensive algal bloom. *J Biogeogr* **43**: 1130–1142.

Grasshoff, K., Kremling, K., and Ehrhardt, M. (1999) *Methods of Seawater Analysis*, 3rd ed. Weinheim, Germany: Wiley-VHC.

Gross, S. (2017) Phenotypic and genotypic responses in the planktonic diatom *Skeletonema marinoi* – Effects of natural processes and anthropogenic stressors. Doctoral thesis. Gothenburg: University of Gothenburg, BrandFactory AB, p 28.

Gross, S., Kourtchenko, O., Rajala, T., Andersson, B., Fernandez, L., Blomberg, A., and Godhe, A. (2018) Optimization of a high-throughput phenotyping method for chain-forming phytoplankton species. *Limnol Oceanogr Methods* **16**: 57–67.

Gruber, N., and Deutch, C. A. (2014) Redfield's evolving legacy. *Nat Geosci* **7**: 853–855.

Guillard, R. R. L. (1975)Culture of phytoplankton for feeding marine invertebrates . In *Culture of Marine Invertebrate Animals*, Smith, W., and Chanley, M. (eds). Boston, MA: Springer, pp. 29–60.

Howarth, R. W., Billen, G., Swaney, D., Townsend, A., Jaworski, N., Lajtha, K., *et al*. (1996) Regional nitrogen budgets and riverine N&P fluxes for the drainages to the North Atlantic Ocean: natural and human influences. *Biogeochemistry* **35**: 75–139.

Hutchins, D. A., and Fu, F. (2017) Microorganisms and ocean global change. *Nat Microbiol* **7**: 17058.

Härnström, K., Ellegaard, M., Andersen, T. J., and Godhe, A. (2011) Hundred years of genetic structure in a sediment revived diatom population. *Proc Natl Acad Sci USA* **108**: 4252–4257.

Kamp, A., Stief, P., Bristow, L. A., Thamdrup, B., and Glud, R. N. (2016) Intracellular nitrate of marine diatoms as driver of anaerobic nitrogen cycling in sinking aggregates. *Front Microbiol* **7**: 1669.

Kremp, A., Godhe, A., Egardt, J., Dupont, S., Suikkanen, S., Casabianca, S., and Penna, A. (2012) Intraspecific variability in the response of bloom-forming marine microalgae to changed climate conditions. *Ecol Evol* **2**: 1195–1207.

McCarthy, J. K., Smith, S. R., McCrow, J. P., Tan, M., Zheng, H., Beeri, K., *et al*. (2017) Nitrate Reductase knockout uncouples nitrate transport from nitrate assimilation and drives repartitioning of carbon flux in a model pennate diatom. *Plant Cell* **29**: 2047–2070.

McQuoid, M. R., Godhe, A., and Nordberg, K. (2002) Viability of phytoplankton resting stages in the sediments of a coastal Swedish fjord. *Eur J Phycol* **37**: 191–201.

Mejía, L. M., Isensee, K., Méndez-Vicente, A., Pisonero, J., Schimizu, N., González, C., *et al*. (2013) B content and Si/C ratio from cultured diatoms (*Thalassirosia pseudonana* and

Thalassirosira weissflogii): relationship to sea water pH and carbon acquisition. *Geochim Cosmochim Acta* **123**: 322–337.

Montoya, J. P., Voss, M., Kähler, P., and Capone, D. G. (1996) A simple high-precision, high sensitivity tracer assay for N_2 fixation. *Appl Environ Microb* **62**: 986–993.

Nelson, D. M., Tréguer, P., Brzezinski, M. A., Leynaert, A., and Quéguiner, B. (1995) Production and dissolution of biogenic silica in the ocean – revised global estimates, comparison with regional data and relationship to biogenic sedimentation. *Glob Biogeochem Cycle* **9**: 359–372.

Olenina, I., Hajdu, S., Edler, L., Andersson, A., Wasmund, N., Busch, S., et al. (2006) Biovolumes and size-classes of phytoplankton in the Baltic Sea. In *HELCOM Baltic Sea Environment Proceedings* **106**: 144.

Redfield, A. C. (1934) On the proportions of organic derivations in sea water and their relation to the composition of plankton . In *James Johnstone Memorial Volume*, Daniel, R. J. (ed). Liverpool, UK: University Press, pp. 176–192.

Redfield, A. C. (1958) The biological control of chemical factors in the environment. *Am Sci* **46**: 205–221.

Rynearson, T. A., and Armbrust, E. V. (2005) Maintenance of clonal diversity during a spring bloom of the centric diatom *Ditylum brightwelli*. *Mol Ecol* **14**: 1631–1640.

Schnetger, B., and Lehners, C. (2014) Determination of nitrate plus nitrite in small volume marine water samples using vanadium(III)chloride as a reduction agent. *Mar Chem* **160**: 91–98.

Sildever, S., Sefbom, J., Lips, I., and Godhe, A. (2016) Competitive advantage and higher fitness in native populations of genetically structure planktonic diatoms. *Environ Microbiol* **18**: 4403–4411.

Sjöqvist, C., and Kremp, A. (2016) Genetic diversity affects ecological performance and stress response of marine diatom populations. *ISME J* **10**: 2755–2766.

Torres, M. E., Mix, A. C., and Rugh, W. D. (2005) Precise d13C analysis of dissolved inorganic carbon in natural waters using automated headspace sampling and continuous-flow mass spectrometry. *Limnol Oceanogr Methods* **3**: 349–360.

Zinner, E., Ming, T., and Anders, E. (1989) Interstellar SIC in the Murchison and Murray meteorites – isotopic composition of Ne, Xe, Si, C, and N. *Geochim Cosmochim Acta* **53**: 3272–3290.

Supporting Information

Additional Supporting Information may be found in the online version of this article at the publisher's web-site:

Text S1. Additional results including clone-specific measurements by EA-IRMS, the third experiment, chain lengths, nutrient conditions and stoichiometry.

Fig. S1. Dissolved inorganic nitrate (a and b), ammonium (c and d), silicate (e and f) and phosphate (g and h) concentrations (μM) under nitrate-replete (a, c, e and g) and nitrate-limited conditions (b, d, f and h) for all clones.

$N = 5$, error bars indicate standard deviation.

Fig. S2. Growth demonstrated by relative fluorescence unit (RFU) at $\log_2$ scale (a and b) and linear scale (c and d), and cells ml^{-1} × 10^3 (e and f), under nitrate-replete (a, c and e)

and nitrate-limited (b, d and f) conditions for all clones, where dotted rectangles mark the 24-h isotope incubations, at exponential (Expo), stationary (Stat) and late stationary (Late) growth phases.

$N = 3–5$, error bars indicate standard deviation.

Fig. S3. Cellular biovolumes.

Average biovolumes (μm^3 cell^{-1}) of *Skeletonema marinoi* from microscopy analyses under nitrate-replete and nitrate-limited conditions for old and young clones.

$N = 5$ and the data are shown as box-whisker plots where median values are shown, with the lower and upper box limits showing the 25th and 75th percentiles, respectively, and whiskers showing the range between minimum and maximum values.

Fig. S4. The clone-specific carbon and nitrate assimilation rates day^{-1} under nitrate-replete (a and c) and nitrate-limited (b and d) conditions during exponential, early stationary and late stationary growth phases, measured by EA-IRMS.

$N = 5$ and error bars indicate standard deviation. Asterisks mark significant differences (*$p < 0.05$, **$p < 0.01$, ***$p < 0.001$) between young and old clones when pooled together, whereby $N = 20$ for all except under nitrate-limited conditions during the exponential growth phase when $N = 15$ for old clones and carbon assimilation and $N = 16$ for young clones for both carbon and nitrate assimilations, due to technical constraints.

Fig. S5. Chain length of *Skeletonema marinoi.* Chain length (cells chain^{-1}) from microscopy analyses of old and young clones of *S. marinoi* under nitrate-limited conditions, during exponential and stationary growth phases.

$N = 5$, error bars indicate standard deviation.

Fig. S6. Dissolved inorganic nitrate concentrations (μM) under nitrate-limited conditions at a high time-resolution for all clones until the nitrate concentration was close to nondetectable after 5 days.

$N = 3$, error bars indicate standard deviation.

Table S1. Growth rates of particulate organic carbon (POC) and nitrogen (PON) at a clone-specific level measured by EAIRMS and C- and N-growth rates at cell-specific levels during the exponential growth phase measured by SIMS. Rates are shown for old (O) and young (Y) clones under nitrate replete and limited conditions.

Table S2. Carbon (C)- and nitrogen (N)-specific growth rate under nitrate-replete conditions at exponential growth phase and nitrate-limited conditions at exponential and stationary growth phase, based on individual cell measurements by SIMS (mean ± SD). $N = 56–265$ cells per strain.

Table S3. Clone-specific particulate organic matter (POM) ratios for carbon (C), nitrogen (N) and phosphorus (P) and clone-specific carbon-to-nitrate assimilation ratios (mol). If available, ratios are included for nitrate-replete and nitrate-limited conditions for the exponential (Expo), stationary (Stat) and late stationary (Late) growth phases. Bold numbers with asterisks mark significantly higher ratios in old (O) or young (Y) clones pooled, where $N = 20$ for all except for numbers marked with plus ($N = 15$) or minus ($N = 16$) due to technical constraints.

Table S4. Particulate organic carbon (POC), nitrogen (PON) and phosphorus (POP) concentrations in μM for all

clones under nitrate-replete and nitrate-limited conditions. If available, concentrations are included for the exponential (Expo), stationary (Stat) and late stationary (Late) growth phases. Bold numbers with asterisks mark significantly higher concentrations in young (Y) or old (O) clones when pooled, where $N = 20$ for all except for numbers marked with a plus ($N = 15$) or minus ($N = 16$) symbol due to technical constraints.

Table S5. Dissolved inorganic nitrate concentrations (μM) for days (D) 0, 4 and 6 under nitrate-limited conditions at a high time resolution. The particulate organic nitrogen (PON) concentration at day 4 (D4) and day 6 (D6) (μM) and the % increase PON concentration between the days. The particulate organic carbon (POC) concentration at D4 and D6 (μM) and the % increase between the days, as well as POC:PON ratios (mol: mol) for D4 and D6 for young (Y) and old (O) clones ($N = 3$).